Research Article | Vol. 25, No. 15 | 24 Jul 2017 | OPTICS EXPRESS 17271
Optics EXPRESS

Enhancement of THz generation by feedback-optimized wavefront manipulation

J. Hah,[1] W. Jiang,[2] Z-H. He,[1] J. A. Nees,[1] B. Hou,[1] A. G. R. Thomas,[1] and K. Krushelnick[1,*]

[1] *Center for Ultrafast Optical Science, University of Michigan, Ann Arbor, MI 48109 USA*
[2] *School of Physical Electronics, University of Electronic Science and Technology of China, Chengdu, Sichuan, China*
[*] *kmkr@umich.edu*

Abstract: We apply active feedback optimization methods to pyroelectric measurements of a THz signal generated by four wave mixing in air using 1 mJ to 12 mJ, 35 fs laser pulses operating at ½ kHz repetition rate. A genetic algorithm, using the THz signal as a figure of merit, determines the voltage settings to a deformable mirror and results in up to a 6 fold improvement in the THz signal compared with settings optimized for the best focus. It is possible to optimize for different THz generation processes using this technique.

OCIS codes: (260.5210) Photoionization; (300.6270) Spectroscopy, far infrared; (320.7120) Ultrafast phenomena; (350.5400) Plasmas.

References and links

1. M. Kreß, T. Löffler, S. Eden, M. Thomson, and H. G. Roskos, "Terahertz-pulse generation by photoionization of air with laser pulses composed of both fundamental and second-harmonic waves," Opt. Lett. **29**, 1120–1122 (2004).
2. T. Bartel, P. Gaal, K. Reimann, M. Woerner, and T. Elsaesser, "Generation of single-cycle THz transients with high electric-field amplitudes," Opt. Lett. **30**, 2805–2807 (2005).
3. X. Xie, J. Dai, and X.-C. Zhang, "Coherent control of THz wave generation in ambient air," Phys. Rev. Lett. **96**, 075005 (2006).
4. K. Y. Kim, J. H. Glownia, A. J. Taylor, and G. Rodriguez, "Terahertz emission from ultrafast ionizing air in symmetry-broken laser fields," Opt. Express **15**, 4577–4584 (2007).
5. H. Roskos, M. Thomson, M. Kreß, and T. Löffler, "Broadband THz emission from gas plasmas induced by femtosecond optical pulses: From fundamentals to applications," Laser Photon. Rev. **1**, 349–368 (2007).
6. K. Y. Kim, A. J. Taylor, J. H. Glownia, and G. Rodriguez, "Coherent control of terahertz supercontinuum generation in ultrafast laser-gas interactions," Nat. Photon. **2**, 605–609 (2008).
7. A. V. Borodin, N. A. Panov, O. G. Kosareva, V. A. Andreeva, M. N. Esaulkov, V. A. Makarov, A. P. Shkurinov, S. L. Chin, and X.-C. Zhang, "Transformation of terahertz spectra emitted from dual-frequency femtosecond pulse interaction in gases," Opt. Lett. **38**, 1906–1908 (2013).
8. X.-Y. Peng, C. Li, M. Chen, T. Toncian, R. Jung, O. Willi, Y.-T. Li, W.-M. Wang, S.-J. Wang, F. Liu, A. Pukhov, Z.-M. Sheng, and J. Zhang, "Strong terahertz radiation from air plasmas generated by an aperture-limited gaussian pump laser beam," Appl. Phys. Lett. **94**, 101502 (2009).
9. D. Kuk, Y. J. Yoo, E. W. Rosenthal, N. Jhajj, H. M. Milchberg, and K. Y. Kim, "Generation of scalable terahertz radiation from cylindrically focused two-color laser pulses in air," Appl. Phys. Lett. **108**, 121106 (2016).
10. H. W. Babcock, "The possibility of compensating astronomical seeing," Publ. Astron. Soc. Pac. **65**, 229–236 (1953).
11. F. Eisenhauer, R. Schödel, R. Genzel, T. Ott, M. Tecza, R. Abuter, A. Eckart, and T. Alexander, "A geometric determination of the distance to the galactic center," Astrophys. J. Lett. **597**, L121 (2003).
12. O. Albert, H. Wang, D. Liu, Z. Chang, and G. Mourou, "Generation of relativistic intensity pulses at a kilohertz repetition rate," Opt. Lett. **25**, 1125–1127 (2000).
13. Z. H. He, B. Hou, V. Lebailly, J. A. Nees, K. Krushelnick, and A. G. R. Thomas, "Coherent control of plasma dynamics," Nat. Commun. **6**, 7156 (2015).
14. A. C. Englesbe, Z. He, J. A. Nees, A. G. Thomas, A. Schmitt-Sody, and K. Krushelnick, "Control of the configuration of multiple femtosecond filaments in air by adaptive wavefront manipulation," Opt. Express **24**, 6071–6082 (2016).
15. H. Hamster, A. Sullivan, S. Gordon, W. White, and R. W. Falcone, "Subpicosecond, electromagnetic pulses from intense laser-plasma interaction," Phys. Rev. Lett. **71**, 2725–2728 (1993).
16. H. Hamster, A. Sullivan, S. Gordon, and R. W. Falcone, "Short-pulse terahertz radiation from high-intensity-laser-produced plasmas," Phys. Rev. E **49**, 671–677 (1994).
17. H. Hamster and R. W. Falcone, "Proposed source of sub-picosecond far infrared radiation," in *Ultrafast Phenomena VII Proceedings of the 7th international Conference*, C. B. Harris, E. P. Ippen, G. A. Mourou and A. H. Zewail, eds. (Springer, 1990) pp. 125–127.

#292263 https://doi.org/10.1364/OE.25.017271
Journal © 2017 Received 6 Apr 2017; revised 24 May 2017; accepted 25 May 2017; published 11 Jul 2017

Optics EXPRESS

18. W. P. Leemans, C. G. R. Geddes, J. Faure, C. Tóth, J. van Tilborg, C. B. Schroeder, E. Esarey, G. Fubiani, D. Auerbach, B. Marcelis, M. A. Carnahan, R. A. Kaindl, J. Byrd, and M. C. Martin, "Observation of terahertz emission from a laser-plasma accelerated electron bunch crossing a plasma-vacuum boundary," Phys. Rev. Lett. **91**, 074802 (2003).
19. J. van Tilborg, C. Schroeder, C. Filip, C. Tóth, C. Geddes, G. Fubiani, E. Esarey, and W. Leemans, "Terahertz radiation as a bunch diagnostic for laser-wakefield-accelerated electron bunches" Phys. Plasmas **13**, 056704 (2006).
20. D. J. Cook and R. M. Hochstrasser, "Intense terahertz pulses by four-wave rectification in air," Opt. Lett. **25**, 1210–1212 (2000).
21. D. J. Cook, J.-X. Chen, and R. M. Hochstrasser, "An intese broadband terahertz source based on a novel four wave rectification process," in *Ultrafast Phenomena XII Proceedings of the 12th International Conference*, T. Elsaesser, S. Mukamel, M. M. Murnane, and N. F. Scherer, eds. (Springer, 2001) pp. 197–199.
22. H.-C. Wu, J. M. ter Vehn, and Z.-M. Sheng, "Phase-sensitive terahertz emission from gas targets irradiated by few-cycle laser pulses," New J. Phys. **10**, 043001 (2008).
23. L. Bergé, S. Skupin, C. Köhler, I. Babushkin, and J. Herrmann, "3D numerical simulations of THz generation by two-color laser filaments," Phys. Rev. Lett. **110**, 073901 (2013).
24. A. Debayle, L. Gremillet, L. Bergé, and C. Köhler, "Analytical model for thz emissions induced by laser-gas interaction," Opt. Express **22**, 13691–13709 (2014).
25. N. V. Vvedenskii, A. I. Korytin, V. A. Kostin, A. A. Murzanev, A. A. Silaev, and A. N. Stepanov, "Two-color laser-plasma generation of terahertz radiation using a frequency-tunable half harmonic of a femtosecond pulse," Phys. Rev. Lett. **112**, 055004 (2014).
26. V. A. Andreeva, O. G. Kosareva, N. A. Panov, D. E. Shipilo, P. M. Solyankin, M. N. Esaulkov, P. González de Alaiza Martínez, A. P. Shkurinov, V. A. Makarov, L. Bergé, and S. L. Chin, "Ultrabroad terahertz spectrum generation from an air-based filament plasma," Phys. Rev. Lett. **116**, 063902 (2016).
27. C. D'Amico, A. Houard, M. Franco, B. Prade, A. Mysyrowicz, A. Couairon, and V. T. Tikhonchuk, "Conical forward thz emission from femtosecond-laser-beam filamentation in air," Phys. Rev. Lett. **98**, 235002 (2007).
28. C. Hauri, W. Kornelis, F. Helbing, A. Heinrich, A. Couairon, A. Mysyrowicz, J. Biegert, and U. Keller, "Generation of intense, carrier-envelope phase-locked few-cycle laser pulses through filamentation," Appl. Phys. B **79**, 673–677 (2004).
29. F. Théberge, W. Liu, P. T. Simard, A. Becker, and S. L. Chin, "Plasma density inside a femtosecond laser filament in air: Strong dependence on external focusing," Phys. Rev. E **74**, 036406 (2006).
30. J. Xie, W.-H. Fan, and X. Chen, "Systematic experimental study on a highly efficient terahertz source based on two-color laser-induced air plasma," Laser Phys. **26**, 055002 (2016).

1. Introduction

Due to increasing demand for electromagnetic waves in the terahertz (THz) range in various fields from biomedical imaging to scientific pump-probe experiments, there have been many efforts to generate a strong THz. The method of using a laser induced plasma as a medium has been highlighted because plasma can be used at intensities well above the damage threshold of nonlinear crystals or semiconductors. Over the last two decades, investigators have shown that including a second harmonic signal in the driving laser field can enhance THz generation [1–7]. Recently, Xie *et al.* [3] delivered frequency doubled beams (2ω) time delayed with respect to the original pulse beam (ω), and Peng *et al.* [8] also used an adjustable aperture to tailor the Gaussian beam to obtain enhanced THz radiation. Another study [9] showed that the energy conversion efficiency of the second harmonic method can be improved using a cylindrical lens. This changes the focal spot and the shape of the filament, improving the structure of the photocurrent within the filament and controllability of the radiation pattern and generation efficiency. For these two-color techniques, the fundamental field and its second harmonic are viewed here as being mixed in air, producing a directional current that drives THz radiation within the timescale of the laser pulse [4]. The spectral extent of the directional current depends on the original spatio-temporal laser fields, which means that the radiated THz spectrum can be modified by manipulating the laser pulse using adaptive optics.

While adaptive optics is new to the generation of strong THz radiation, it has been widely used for improving optical systems degraded by environmental effects [10, 11]. Numerous laser-driven plasma sources have employed genetic algorithms (GA) to optimize the desired outcomes [12–14]. In this paper, we use a deformable mirror and active feedback to enhance THz signals produced by two different processes by up to 6 fold over un-optimized results.

Optics EXPRESS

2. THz generation mechanism from laser-induced plasma

Following Hamster *et al.* [15, 16], laser-induced plasma has been widely used for generating a strong THz radiation. A plasma wake excitation mechanism was introduced to explain the generation mechanism of THz [17]. In this model, the ponderomotive force induced by an intense laser pulse results in the production of a plasma wave that generates strong THz electromagnetic radiation. For high laser powers, a related mechanism is coherent transition radiation from a laser wakefield accelerator (LWFA) [18,19]. When the electron propagates through the plasma-vacuum interface generated by the LWFA, it emits transition radiation, which interferes coherently for wavelengths longer than the electron bunch length.

To enhance the THz radiation for lower levels of input laser energy (< 1mJ), a frequency-doubled beam was introduced to the fundamental beam. This second harmonic method can enhance THz generation by more than 100 times [20, 21]. A number of studies using the second harmonic method have revealed other THz generation mechanisms [1–7]. Among many suggested theories, the two most well-known are the four wave optical rectification model [1–3, 20] and the photocurrent model [4, 6, 22, 23].

In the first theory, when the two beams interact within an air-breakdown plasma, which is a nonlinear medium, the THz radiation is generated and rectified by the four-wave mixing phenomenon. This is related to the third order nonlinearity $\chi^{(3)}$ ($\Omega_{THz} : 2\omega + \Omega_{THz}, -\omega, -\omega$). However, the four wave mixing theory based on the third order nonlinearity ($\chi^{(3)}{}_{\text{ions}}$ or/and $\chi^{(3)}{}_{\text{free electrons}}$), cannot explain the observed THz field. Therefore, a photocurrent model was proposed by Kim *et al.* [4] In this model, when the two laser beams are mixed with the proper phase difference, the bound electrons are stripped off by an asymmetric laser field. These electrons then produce a non-vanishing transverse plasma current $j_\perp = -n_e e v_e$, where n_e is the electron density, and v_e is the electron velocity in a laser field. Within the timescale of the photoionization, the burst of photocurrent produces THz radiation.

Recently, many studies have shown that broadband THz spectra generated by the second harmonic method have multiple origins depending on their frequency range [7, 24–26]. In the low frequency region (1 THz to 5 THz), the free-electron photocurrent is the major contribution to THz radiation. As the frequency increases beyond 5 THz, the Kerr nonlinear response of the neutral molecules, which is related to four wave mixing, dominates.

3. Experimental setup

Our experiments were performed using the Lambda-Cubed (λ^3) laser facility at the University of Michigan. λ^3 is a Ti:Sapphire system (central wavelength λ=800 nm) producing laser pulses with τ=35±2 fs FWHM duration. The system, operating at ½ kHz, delivers 1 to 12 mJ pulses onto a 0.1 mm thick Beta Barium Borate (BBO) frequency doubling crystal to produce the asymmetric laser field required for the two-color THz radiation generation method. The laser pulses are focused by an $f/15$ lens to an interaction point where plasma filaments are generated, 25 cm behind a BBO crystal. A silicon window of thickness 5 mm filters the two laser fields (800 nm and 400 nm), allowing only the THz field to pass. The THz field is subsequently collimated by an $f/6$, 90° parabolic reflector. It is relayed by a pair of parabolic mirrors to a Michelson interferometer and is refocused by a final parabolic mirror onto a pyroelectric detector (Gentec-EO, QS-IL). A commercial nitrocellulose pellicle (Thorlabs BP245B2) is used as a beam splitter. The experimental configuration is shown in Fig. 1.

Laser pulses are delivered to the BBO frequency doubling crystal, experience distortion due to air turbulence and optical imperfections. To compensate for these defects and also to optimize the THz yield, the 50 mm beam first impinges on a deformable mirror and then focuses via the $f/15$ lens to generate plasma filaments.

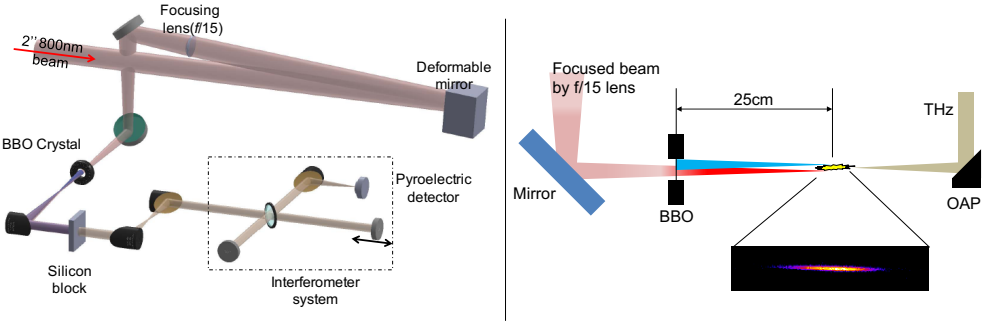

Fig. 1. (Left) The experimental setup including a deformable mirror. The deformable mirror is controlled by a computer with the LabVIEW software. (Right) Corrected beam (800 nm, red in the figure) is focused by $f/15$ lens. To generated 400 nm beam (blue in the figure), a BBO crystal is located at 25 cm before the geometric focus.

3.1. Deformable mirror and genetic algorithm

The deformable mirror used for our experiment consists of a silver coated glass surface with 37 electrostrictive actuators supporting the sheet. These actuators are controlled by 37 independent voltage values: one for each actuator, to find the best mirror shape for the best THz yields, correcting wavefront distortions caused by air flow or imperfections on optics. Note that the correction procedure may include not only eliminating unwanted wavefront distortions, but also adding desired imperfections. The maximum stroke range of the actuator is 4 μm for 100 V applied voltage [13, 14]. The genetic algorithm is a stochastic parallel algorithm technique analogous to the process of natural selection in evolutionary biology. This method was developed for solving global optimization problems in complex system with a large number of variables. One can apply deformable mirror shapes to optimize a figure of merit (FOM) based on the experimental signal. In our experiment, we choose the THz yield (represented by the pyroelectric detector voltage) as a feedback signal to enhance the THz field strength. The genetic algorithm generates 10 "parent" settings, and from each "parent" setting, 10 mutated "offspring". With these 10 parents and 100 offspring mirror settings, the algorithm evaluates 110 different mirror figures, and computes a single-valued FOM to rank the generation. The top 10 results are assigned as new "parents" for the next generation and the mutation and evaluation are repeated. Optimization is performed at various pulse energy.

3.2. THz detection and spectrum analysis

The THz field was detected by a pyroelectric detector after passing by a silicon window and a Michelson interferometer. The calibrated detector sensitivity was 3.7×10^5 V/J. The maximum measured THz signal was found to be 260 nJ per pulse with a conversion efficiency of 0.004 %. The measured signals under different conditions are described in Fig. 4.

A computer controlled translation stage with 0.1 μm step size is used to scan the Michelson interferometer to determine the THz spectrum by Fourier transform spectroscopy. In the interferometric measurements, we experience a signal variation due to acoustic effects, because the air-breakdown causes an acoustic signal that vibrates the pellicle. During optimization, the acoustic signal level varies slightly for each mirror shape generated by the genetic algorithm. To reduce the signal variation, we built a box around the interferometer to limit the vibration and, also enclosed the THz generation region in a foam tube to minimize microphonic effects in the pyroelectric detector.

Optics EXPRESS

4. Results and discussion

At the beginning of the experiment, all 37 actuators are set to 0 V, i.e. relatively flat mirror shape for manual alignment. When the genetic algorithm starts to optimize the output signal, the system applies 30 V to all actuators and "mutates" each actuator voltage from the that setting. The signal improvement through 41 generations for 1.2 mJ of incident energy is shown in Fig. 2, where the x-axis represents the generation of the GA, and the y-axis shows the signal relative to the starting point. Figure 2 shows the 10 best "offspring" for each generation. For the 1st generation, the 10 results are the mutations of the 30 V parents. Because the GA has no preference for mutations, the first 10 mutations can generate both favorable mirror shapes, and worse mirror shapes. Therefore, Fig. 2 also shows lower-than-unity FOM values for the 1st generation (0.15 to 0.91). But, after the 1st generation, the GA proceeds to find better results with consistent improvement. After the 41st generation, the maximum signal is 2.4 times higher than the FOM of the original 30 V mutations. This performance is consistent from run to run, though the particular mirror shapes are not necessarily repeated. For the THz yield, we obtained a 5.6 mV signal with the best output mirror shape, which corresponds to a 2.4 times improvement in THz yield relative to the 30 V mirror shape (2.3 mV). We produced the same level of THz signal improvement months later, from the same setup: measuring 2.1 mV and 5.1 mV respectively. Repeating experiment with a 3 mJ incident energy, we obtained 4.8 times improvement.

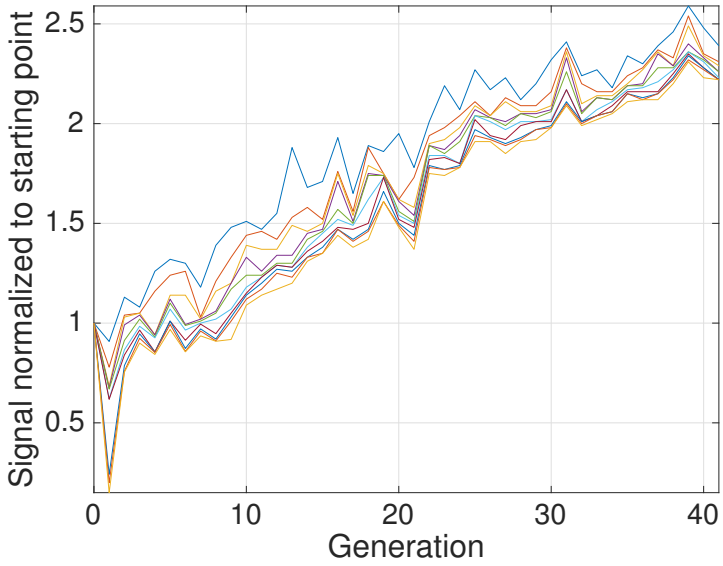

Fig. 2. Signal improvement through 41 generations for 1.2 mJ incident pulse energy.

From the Michelson interferometry of the THz radiation, we perform spectral analysis using a Fourier transform spectroscopy, and it is shown in Fig. 3. In these graphs, the red lines show the interferogram and spectrum prior to optimization, and the blue lines show the results with the optimized mirror shape. The peak-to-valley difference in the interferogram increases from 3.4 mV to 5.8 mV, and the bottom graph shows the THz spectrum improvement from 1 THz to 70 THz, with the signal doubling between 5 THz and 40 THz. In these frequency ranges, the generation of THz is affected by four wave mixing theory, indicating that our system improves the THz yields by modifying the Kerr nonlinear response of the neutral molecules. Note that for the low frequency range (<5 THz), there is strong attenuation due to water vapor in the air [27].

Optics EXPRESS

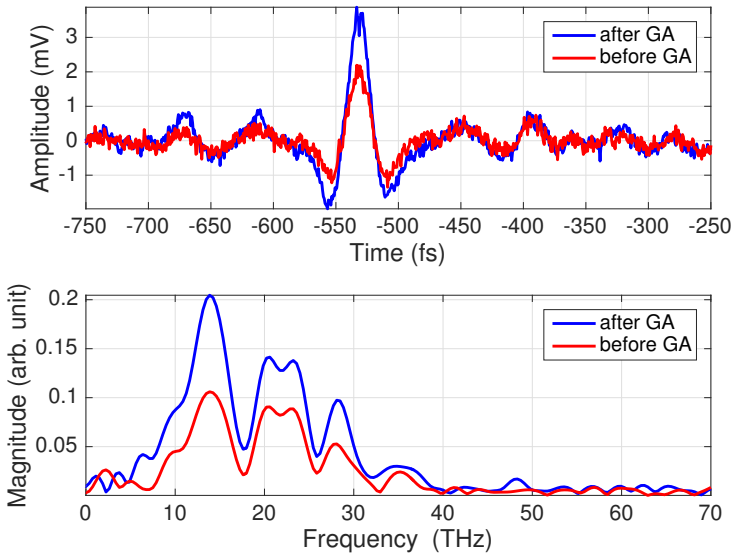

Fig. 3. (Top) Two interferograms before(red)/after(blue) optimization (Bottom) Spectrum analysis.

Taken together, these results indicate that our active feedback system optimizes the mirror figure for enhanced THz generation correcting for defects in the whole optical system. This includes imperfections such as air turbulence and accounts for the details of the phase figure needed to maximize the THz generation via Kerr effects. Here, the optimal mirror shape is the best *time-averaged* figure for THz generation in the presence of air turbulence. This differs from astronomical applications which offer *real-time corrections* for air turbulence.

We also characterize the THz yield with varying input pulse energy. There are two main experimental factors for determining the THz yield: 1) the use of the BBO crystal, 2) the optimization through the GA. Ideally, an optimization would be done at the desired laser energy. However, the random mirror shapes generated during the GA could make hotspots on the beam profile, causing damage on the BBO crystal. To avoid damage, the optimization process is done at a lower energy (3 mJ, optimization point #1 in Fig. 4), then, the resulting mirror shape is applied to generate THz radiation at higher energies. In this experiment, the THz signal increases 5 fold as a result of optimization, retaining greater than a 3 fold improvement between energy levels 2 mJ to 6.2 mJ.

Without the BBO crystal, damage is no longer a consideration, and the optimization process can be done with moderate incident energies (e.g. 6.4 mJ, optimization point #2 in Fig. 4) and the resulting mirror shape is applied to other energy levels showing the scalability of the solution. In the single-color case (without the BBO), the THz generation mechanism is different than two-color case. The source of the far-field THz radiation is the set of plasma waves generated due to the propagation of the laser through the atmosphere [15, 16]. Thus, the THz emission we optimized using the single-color method is likely due to the optimization of the plasma wave amplitude. This mechanism is more dependent on having the correct temporal pulse shape, and also having a focal spot similar in dimensions to the relativistic plasma wavelength. The relativistic plasma wavelength is a function of the electron density which is determined by the laser intensity. The amplitude of the plasma wave can also be improved if there are temporal structures in the driving laser pulse which are less than the plasma period. So the focal spot and

Optics EXPRESS

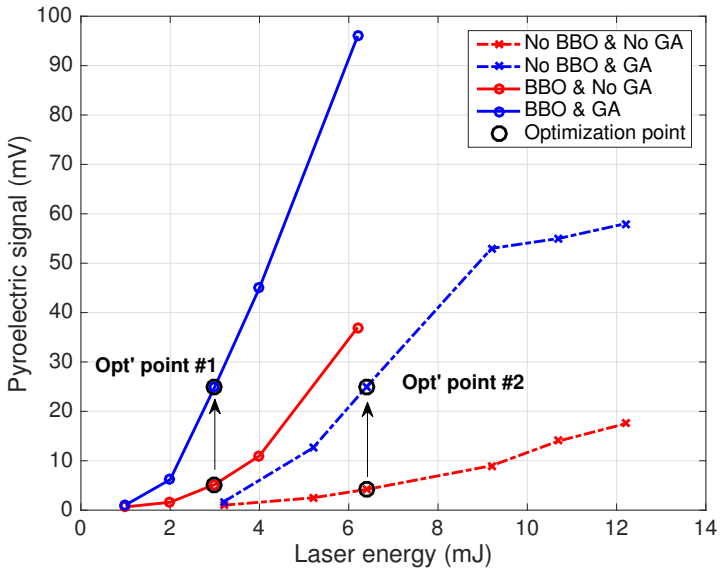

Fig. 4. THz energy measurements with a pyroelectric detector. THz emission is measured at 4 different situations. Dotted lines represent single-color results and solid lines show two-color results. Red and Blue color represent before/after optimization results, respectively. For the two-color case (Opt' point #1), optimization process was done at 3 mJ, and it required 99 generations, and 6.2 mJ and 47 generations for the single-color case(Opt' point #2). Note that the pyroelectric detector sensitivity was 3.7×10^5 V/J. The maximum THz energy was 260 nJ per pulse with an input energy of 6.2 mJ, resulting in the conversion efficiency of 0.004 %

the electron density are connected in a complicated way that also depends on pulse energy. Note that the temporal shape of the laser pulse is also affected by the filamentation process [28]. Thus, the shape of the plasma wave which optimizes the THz generation for the single-color method is not the same as that for the second harmonic method, and in these experiments, the optimized phase front of the single-color case is clearly different than that of the two-color case.

Figure 5 shows four optimized mirror shape illustrations for different THz generation mechanisms and pulse energies. It is clear that these mirror shapes will produce different focal spot structures. However, it should be noted that for the same pulse energy and generation mechanism, although the precise mirror shape may differ from experiment to experiment, the amount of THz produced after mirror optimization is generally reproducible. Using the two-color method, diagonal voltage patterns are observed on the deformable mirror which cause the mirror to form a slightly cylindrical shape, thus generating a slight “line-focus" (see Fig. 5 (c) and (d)). This focal spot structure is also not along the direction of laser polarization. By contrast, in the single-color case (without the BBO crystal), no distinct patterns of mirror deformation emerge. This suggests that a more complex and larger focal spot is produced such that the path lengths from various parts of the beam may result in pulse modulation. From these mirror shapes, it is clear that the presence of the BBO crystal has changed the wavefront of the optimized laser pulses significantly which results from optimization for a different THz generation mechanism. It is also clear that the focal spot structure that optimizes the THz production for a particular energy is not the same as that which optimizes THz production at other pulse energies. This is precisely because of the complex 3D self-focusing and diffraction effects involved in the filamentation process. As the energy of the pulse is increased, the amount of mirror deformation required for optimum

Optics EXPRESS

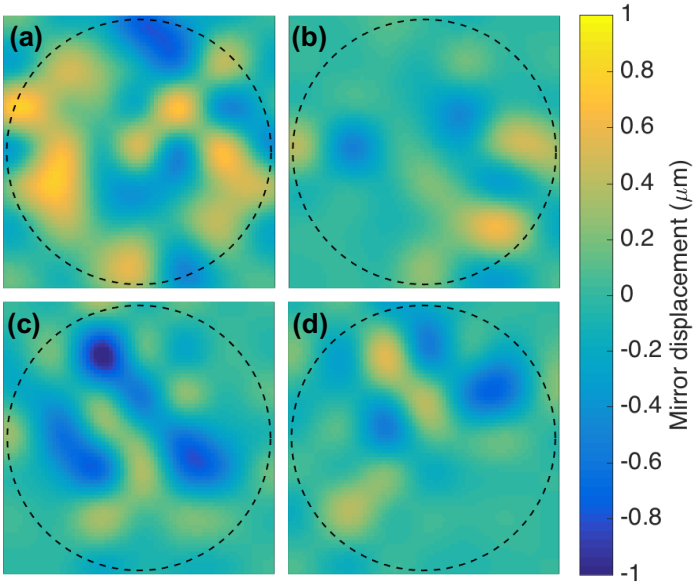

Fig. 5. Various result mirror shape illustrations from different optimization conditions. The images are reconstructed from the applied voltage on electrostrictive actuators. (a) Single-color at 3mJ, (b) single-color at 6mJ, (c) two-color at 1.2mJ, and (d) two-color at 3mJ.

THz enhancement is reduced even though the amount of THz enhancement is similar as at lower energies. This is likely to be because the amount of asymmetry in the focal spot required to“seed" a particular filamentary structure is reduced at higher energies.

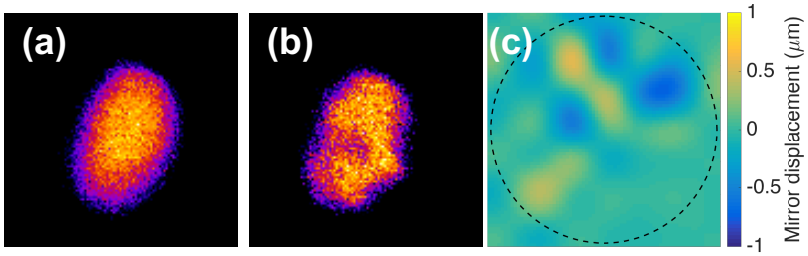

Fig. 6. Beam cross-section image (a) before GA, and (b) after GA. (c) Optimized mirror shape generating the highest THz yield from two-color method after 75 generations. The deformable mirror with voltage distribution (c) changed the beam cross-section from (a) to (b)

Figure 6 shows beam images, taken at the location of the BBO crystal and the optimized mirror shape with a 3 mJ laser input pulse. (a) is the cross-section image of the 0 V mirror (i.e. relatively flat mirror) and (b) is that of the optimized mirror. Compared to (a), the intensity of (b) is lowered in its central region and higher on the lower right side. Figure 6 (c) shows the deformable mirror shape with respect to its surface displacement (μm) for the highest THz yield. The mirror shape indicates that the focal spot is elongated and it does not have a specific geometric shape such as tip/tilt or focus/defocus, because it was identified by selectively testing the various mirror figures applied by the GA. Also, changes in plasma filamentation are observed

Optics EXPRESS

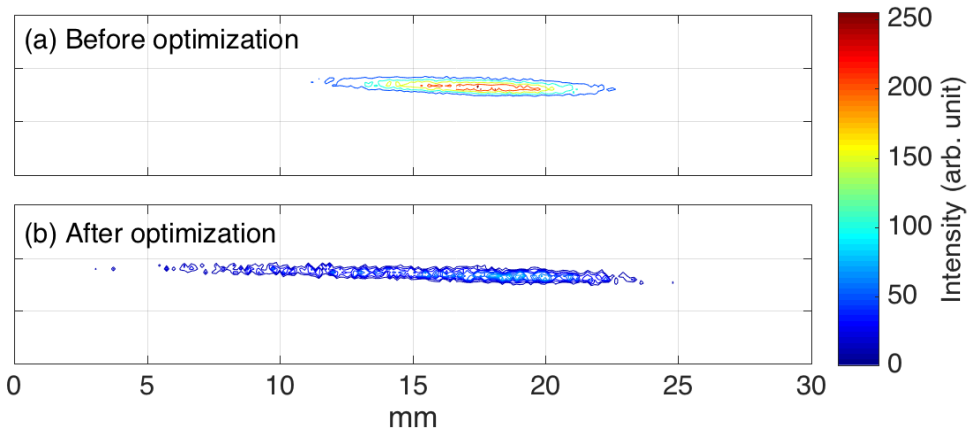

Fig. 7. Plasma filament images, (a) before and (b) after optimization with 1.6 mJ laser input energy. The length of filament is doubled and its intensity decreases. As laser input energy increases, filament length increases up to 100 mm.

during optimization. We found that air-breakdown produced by different mirror shapes generated acoustic signals with varying amplitude and frequency content. It is clear that the optimized focal spot is larger since the images from side scattering are much less intense and the sounds from the breakdown are much reduced. Figure 7 shows that the length of the filament doubles and total light emission from filament decreases more than 3 times, denoting larger plasma volumes. The larger plasma volume is known to generate stronger THz signals [29, 30]. Because the laser wavefront experiences great modifications through the plasma filaments, such variations of plasma filament characteristics are the key to understanding THz generation from the laser plasma interaction.

5. Conclusion

In summary, we have adapted an active feedback method using a deformable mirror and a genetic algorithm to improve the output of THz radiation generated by four wave mixing mechanism. The distorted wavefront resulting from air turbulence or defects of the optical components is compensated by a deformable mirror figure obtained by the genetic algorithm. The method finds the optimal spatial-phase configuration of the fundamental light for the generation of THz radiation. This includes implicit manipulation of the phase configuration of both the fundamental and the second harmonic fields, and it yields a significant enhancement in the THz radiation. With the optimal mirror shape on the deformable mirror, the THz signal amplitudes can be improved by 2 to 6 times compared to that before optimization. Using the feedback method, we show that one can optimize different THz configurations even though the generation mechanisms are different. The optimized phase front for the two-color source is not the same as the optimized phase front for the single-color source. Using this technique, one could also optimize the THz signal in a particular wavelength range by controlling the different THz generation mechanisms separately by the advantage of adaptive optics and the feedback system.

Funding

Air Force Office of Scientific Research (AFOSR) (FA9550-12-1-0310); U.S. Department of Energy (DE-SC0008352).